

# Dual phase titanium alloy hot forging process design: experiments and numerical modeling

A. Ducato<sup>1</sup> · G. Buffa<sup>2</sup> · L. Fratini<sup>1</sup> · R. Shivpuri<sup>2</sup>

Received: 27 February 2015 / Accepted: 29 October 2015 / Published online: 28 November 2015  
© Shanghai University and Springer-Verlag Berlin Heidelberg 2015

**Abstract** Titanium alloys are considered desirable materials when both good mechanical properties and weight reduction are required at the same time. This class of materials is widely used in those fields (aeronautics, aerospace) in which common steels and light-weight materials, e.g., aluminum alloys, are not able to satisfy all operative service conditions. During the last decade, forging of titanium alloys has attracted greater attention from both industrial and scientific/academic researchers because of their potential in providing a near net shaped part with minimal need for machining. In this paper, a numerical model of the forging sequences for a Ti-6Al-4V titanium alloy aerospace component is presented. The model was tested and validated against experimental forgings. The model is then applied to predict loads final microstructure and defects of an aeronautical component. In addition to metal flow and die stresses, microstructural transformations ( $\alpha$  and  $\beta$  phases) are considered for the determination of proper process parameters. It is found that transformation from  $\alpha/\beta$  to  $\beta$  phase during forging and reverse transformations in post-forge cooling needs to be considered in the computational model for reasonable prediction of forging loads and product properties.

**Keywords** Finite element method (FEM) · Ti-6Al-4V · Hot forging · Phase prediction

---

✉ A. Ducato  
antonino.ducato@unipa.it

<sup>1</sup> Department of Chemical, Management, Computer and Mechanical Engineering, University of Palermo, Viale delle Scienze, Palermo 90128, Italy

<sup>2</sup> Integrated Systems Engineering, The Ohio State University, 1971 Neil Ave, Columbus, OH 43210, USA

## 1 Introduction

Titanium alloys have higher strength than most steels with only about 60% of the weight. Their lower density allows these alloys to be used in applications where lower weight is a key factor [1]. Furthermore, the corrosion resistance of titanium permits to avoid corrosion protective coatings or painting even in extremely corrosive environments. Finally, the use of polymer matrix composites (PMCs) has significant compatibility problems that limit their larger utilization in aircraft structures. Titanium is galvanically compatible with the carbon fibers in the composites, whereas aluminum (and low alloy steels) generates significant galvanic potential. As for aluminum, these alloys are widely used in components where high strength and low weight are important, and operative characteristics include corrosion resistance and tolerance to high temperatures. In these conditions, titanium alloys show high-performance and versatility. For these reasons, titanium alloys are extensively used for aeronautical components including crankshafts, connecting rods and a variety of drivetrain components.

Titanium has two solid crystalline forms: at low temperatures, the crystalline phase is called Alpha ( $\alpha$ ), and it has a hexagonal closed packed (HCP) structure; at high temperatures, the crystalline phase is called Beta ( $\beta$ ) and has a body centered cubic (BCC) structure. The temperature at which the solid becomes fully  $\beta$  is called  $\beta$ -transus temperature and changes as a function of the alloying elements, ranging from 670 °C to 1 050 °C [2]. The usual composition of the titanium alloys commonly used for forging processes is 70%–100% of pure titanium. The main alloying elements are aluminum (0–6%), tin (0–6%), which work as  $\alpha$  phase stabilizers and cause an increase of  $\beta$ -transus temperature. Vanadium (0–13%),

molybdenum (0–11%), and chromium (0–11%), which are  $\beta$  phase stabilizers and cause a decrease of  $\beta$ -transus temperature. The use of aluminum enables lower density, while all the other alloying elements cause the density to increase. On the other hand, it should be taken into account that the raw material may cost from 3 to 10 times as much as steel or aluminum. A major drawback in the use of titanium alloys is a significant production cost, especially when the production processes are based on machining operations, which are at least 10 times as expensive as machining of aluminum alloys [3]. The machinability of titanium and its alloys is generally considered poor owing to several inherent properties of these materials. In fact, titanium is chemically reactive and, therefore, has a tendency to bond to the cutting tool edge during machining, thus leading to chipping and premature tool failure. In this way, the buy-to-fly ratio, i.e., the ratio between the weight of raw material bought and the weight of the final component, is very high, confining this kind of manufacturing operations to those applications in which the operative conditions of components justify their production costs. Nevertheless, in the actual industrial panorama, aerospace companies are driving the research and development efforts toward new alloys and processes in order to obtain both a significant reduction of costs and a greater sustainability of the production chain. Hot forming processes, such as hot forging or rolling, can help reach these objectives by manufacturing of both semi-finished and finished products resulting in lower values of the buy-to-fly ratio with respect to the current practice [4].

However, titanium and its alloys are rather difficult to form into a complex shape because of their limited forging temperature range due to the large variation of flow stress with temperature and strain rate [5]. Because of the low heat capacity, titanium alloys require heated dies or isothermal forging. Hence, forging processes may be expensive but, at the same time, can provide better product quality, near net shape parts and, consequently, lower machining cost and waste of material. However, the process setup needs a strong knowledge of material properties and behavior in order to choose the best parameters as a function of the specific titanium alloy to be forged and customer needs in terms of final product mechanical properties. In many alloys, the  $\alpha$  phase, which forms on the outer surface of the forged component, has lower ductility and is subject to moderate to severe surface cracking. In general,  $\beta$  alloys are easier to forge than the  $\alpha+\beta$  alloys and  $\alpha$  alloys. Initial forging temperatures for ingot breakdown are higher than the intermediate forging temperatures, which, in turn, are higher than the finish forging temperatures. What is referred to as “conventional forging” occurs at temperatures below the  $\beta$  transus, usually in the  $\alpha+\beta$  region of the alloy. The so called  $\beta$  forging occurs at

temperatures above the  $\beta$  transus. Similarly to other common forging alloys, many titanium alloys show a strain-softening for the strain rate values typically used in conventional forging processes. The material flow stress is mainly influenced by the microstructure. The equiaxed  $\alpha$  in a  $\beta$  matrix structure, typical of forging operations below the  $\beta$ -transus point, redistributes strain and promotes dislocation movement more effectively than acicular  $\alpha$  in a transformed  $\beta$  microstructure, leading to increased strain softening. Forging pressures can significantly exceed the pure flow stress of any given alloy under similar deformation conditions [6] due to the values of a few process variables, i.e., die temperature, lubrication and total strain. In this scenario, a significant help may come from the use of computer aided design techniques, which can assist the designers in the determination of the best process setup. Numerical simulations can show the process evolution in terms of material flow, cavity filling and requested equipment, i.e., forging load [7]. In particular, the most effective set of process parameters, allowing the minimization of energy consumption and maximizing product quality, must be determined. In order to get effective prediction of the final product local mechanical characteristics, numerical modeling of the process needs proper material characterization including thermal, physical and mechanical data, used for conventional coupled thermo-mechanical analyses, as well as metallurgical models [8, 9].

In this paper, a numerical analysis on hot forging of a Ti-6Al-4V component for aeronautical applications is presented. The numerical model was calibrated and validated by means of experimental data coming from previous studies [10]. A dedicated numerical model was used to simulate the process and the metallurgical evolutions occurring during both the forging process and the cool down [10, 11]. Simulations were run under different thermo-mechanical conditions and the final microstructure was predicted. The goal was to determine the effect of initial billet temperature and die geometry on the material flow and microstructural properties of the forged part. All simulations were carried out using the implicit Lagrangian code DEFORM3D<sup>TM</sup>.

## 2 State of the art

A key factor for reliable numerical analysis of forming processes is proper material modeling in terms of flow stress, as a function of the thermo-mechanical field variables evolution. A few researches can be found in literature focusing on the numerical characterization of titanium alloys (especially the Ti-6Al-4V alloy) both from a thermo-mechanical and metallurgical point of view.

Cai et al. [12] presented an investigation on the effects of temperature on flow stress of Ti-6Al-4V alloy during

isothermal hot compression tests over a range of temperatures from 800 °C to 1 050 °C and strain rates from 0.000 5 s<sup>-1</sup> to 1 s<sup>-1</sup>. Experimental data were used to determine a constitutive equation relating flow stress, strain rate and temperature by considering a compensation for strain. Strain was shown to have significant influence on material constants.

Seshacharyulu et al. [13] studied microstructural mechanisms in the hot deformation of commercial Ti-6Al-4V with an equiaxed  $\alpha$ - $\beta$  microstructure by means of tensile tests conducted on cylindrical specimen in a range of temperature from 750 °C to 1 100 °C, and strain rate range from 0.000 3 s<sup>-1</sup> to 100 s<sup>-1</sup>. The material exhibits a wide regime of flow instabilities at strain rates higher than 0.1 s<sup>-1</sup> showing adiabatic shear bands in the  $\alpha$ - $\beta$  range. This region must be avoided in order to obtain the desired microstructure. Moreover, at the  $\beta$ -transus, a high ductility was observed at the strain rate of 0.01 s<sup>-1</sup>, which was attributed to a transient superplasticity mechanism of fine-grained  $\beta$  phase.

Park et al. [5] analyzed the deformation behavior of Ti-6Al-4V titanium alloy by hot compression tests in a temperature range from 850 °C to 1 000 °C and strain rate range from 0.001 s<sup>-1</sup> to 10 s<sup>-1</sup>. Processing maps were generated using unified relationships between constitutive deformation behavior, hot workability and microstructures evolution. The obtained results were implemented into a subroutine developed with the commercial FE code DEFORM2D<sup>TM</sup>. The simulations were carried out to evaluate the flow and microstructure stability for Ti-6Al-4V pancake forgings. The results showed that the highest efficiency of power dissipation was obtained at temperature of 850 °C and strain rate of 10<sup>-3</sup> s<sup>-1</sup>, while unstable regions were observed both with temperature of 850 °C and strain rate of 10 s<sup>-1</sup> and with temperatures higher than 970 °C and strain rates lower than 10<sup>-1</sup> s<sup>-1</sup>.

The incidence of cavity initiation and gross, free-surface, fracture during the sub-transus hot pancake forging of Ti-6Al-4V was studied by Semiatin et al. [14]. Cavity initiation occurred, at temperature close to  $\beta$ -transus point and relatively low strains, in the  $\beta$  phase lying between the grain-boundary  $\alpha$  phase and the lamellar colonies. While, at temperatures near the  $\beta$ -transus, cavity initiation occurred at much greater strains as a result of micro-fracture in the globularized  $\alpha$  phase. The authors used a finite element (FE) analysis to correlate both the cavity initiation and the gross free-surface fracture results. The deformation parameters associated with cavity initiation and free-surface fracture were quantified using numerical techniques, in addition, the damage mechanisms were compared to those previously developed for hot tension testing of Ti-6Al-4V having an identical microstructure. Hu and Dean [15] studied the effects of temperature and strain rate on the forging process of Ti-6Al-4V by means of finite element methods. Both

isothermal and hot-die conditions were tested in order to find an effective method for the production of near-net-shape blades. Comparison between numerical and experimental results showed good agreement.

The microstructural properties of the considered alloy have a significant impact on the quality of the prediction of the material behavior during a hot forging process as both phase and related material properties can change with the thermal and mechanical variables. Geijselaers and Huétink [16] based their research on the creation of a mathematical model used as base for a 2D analysis. The adopted approach allowed the calculation of phase transformations only as function of the thermo-mechanical conditions with the following steps: thermal problem solution; calculation of temperature variations with induced phase changes and thermal loads; mechanical problem solution; calculation of strains and recalculation of temperature and global stress state. The model proposed by Casotto and Pascon [17] is based on a 2D coupled analysis of an industrial ring-rolling process. As opposed to the first model, it took into account the global material behavior during its thermo-mechanical evolution by a proper calibration on the base of all the microstructural evolutions of the considered alloy. Sha and Malinov [18] conducted the fundamental research about the kinetics governing the evolution of microstructure for several titanium alloys, with particular reference to Ti-6Al-4V alloy. Obtained results showed how the phases evolved, starting from the base material conditions ( $\alpha$  and  $\beta$  microstructure), as a function of heating and content of Al and V.

### 3 Materials and methods

The material used for this study is the Ti-6Al-4V alloy, which is the most used titanium alloy in the aerospace industry. The chemical composition of the used alloy is given in Tables 1. Table 2 shows the comparison between the buy to fly ratio of the machined and forged part.

Ti-6Al-4V is a dual phase  $\alpha$ - $\beta$  alloy showing different volume fractions of  $\alpha$  and  $\beta$  phases, depending on heat treatment and interstitial (primarily oxygen) content [19]. Furthermore, Ti-6Al-4V can have a variety of microstructures with different geometrical arrangements of the  $\alpha$  and  $\beta$  phases, depending on the thermo-mechanical conditions reached during the process and subsequent cool down. As far as the as received material was concerned, the microstructure was characterized by  $\alpha$  globular grains in a  $\beta$  matrix (see Fig. 1). The phase volume fractions were 91% and 9%, respectively.

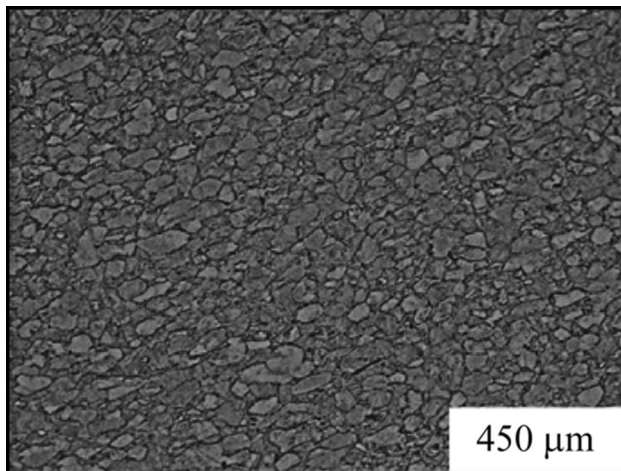
Consequently, the forging conditions, i.e., the maximum temperature experienced, strain and cooling rate, largely influence the mechanical characteristics of the forged components. If plastic deformation occurs in the “ $\beta$

**Table 1** Ti-6Al-4V chemical composition

w(Ti)/%	w(C)/%	w(Fe)/%	w(N)/%	w(Al)/%	w(O)/%	w(V)/%	w(H)/%	w(V)/%	w(other)/%
Balance	0.080	0.030	0.050	5.500– 6.750	0.200	3.500– 4.500	0.015	0.005	0.400

**Table 2** Workpiece and billet volume with buy-to-fly reduction

Machined part volume/mm <sup>3</sup>	Hard machining billet/mm <sup>3</sup>	Forging billet/mm <sup>3</sup>	Hard machining buy/fly	Forging buy/fly	Buy/fly reduction/%
682 442	1 572 744	689 187	2.28	1.01	55.7

**Fig. 1** Microstructure of the as received Ti-6Al-4V alloy

region”, the final microstructure becomes  $\alpha$  lamellar with rough dimension lamellae [5]. When the plastic deformation occurs below the  $\beta$ -transus temperature (about 980 °C), the final microstructure becomes bimodal with small lamellar  $\alpha+\beta$  and  $\alpha$  grains. Hence, the temperature at which the process is carried out also has a strong influence on the forging loads, being the flow stress of the  $\alpha$  phase about three times the one of the  $\beta$  phase [20, 21]. Figure 2 shows the 3D view of the part considered in this study (see Fig. 2a), the as-forged component (see Fig. 2b) and its CAD geometry (see Figs. 2c, d).

The die (see Figs. 3, 4) was properly designed to achieve a satisfactory forged shape using an optimized amount of raw material thus reducing the machining operations required to reach the final geometry.

The forging campaign was carried out using two different temperature levels in order to study the material behavior when both  $\alpha$ - $\beta$  and  $\beta$  field are considered for the initial thermal conditions. The billets were pre-heated at 950 °C and 1 050 °C for  $\alpha$ - $\beta$  and  $\beta$  field forging, respectively, while the initial die temperature was fixed at 400 °C for all the tests.

A hammer press was used to carry out the forging operations in order to prevent critical cooling of billets,

which may produce incorrect material flow with bad cavity filling and incorrect final shape due to the rapid cooling of the areas close to the contact outer surfaces. Dry lubrication was considered. A single step forging was carried out to produce a near net shape part. A cylindrical billet, having diameter of 70 mm and height equal to 170 mm, was used. An industrial hammer press with the maximum energy of 600 kJ was utilized for the experiments. The forged part was cooled down to room temperature in air. After the cooling stage, the workpiece was analyzed in order to compare the results of the numerical code from both a die-filling and microstructural point of view. In order to characterize the microstructure, the experimental volume fraction of the different phases was determined using a specific and properly calibrated image analysis software [22]. Optical micrographic images of the cross section of the forged parts were used for the image analysis procedure. The images were acquired after hot mounting, fine grinding, polishing and finally etching with Keller reagent for 15 s of the specimen taken in the same reference points described in the following paragraph.

The proposed approach resulted in a dramatic reduction of the theoretical amount of material needed with respect to the hard machining approach. The raw material needed for the two approaches is shown in Table 1.

The commercial implicit Lagrangian code DEFORM3D™ was used for the numerical simulation. The  $\alpha$  phase to the  $\beta$  phase transformation during heating up was modeled through the simplified form of the Avrami model which was embedded in the utilized code. The transformation from the  $\beta$  phase to the  $\alpha+\beta$  phase during cooling down was modeled using the TTT curves for the used material. It should be observed that TTT curves can be utilized instead of the more correct CCC curves considering that during the extremely small time steps used for the simulation small temperature changes take place and almost isothermal conditions are found. The full details of the equations and coefficients utilized can be found in Ref. [23], in which the calibration of the model was carried out for the friction stir welding process of the same Ti-6Al-4V titanium alloy used in this study.

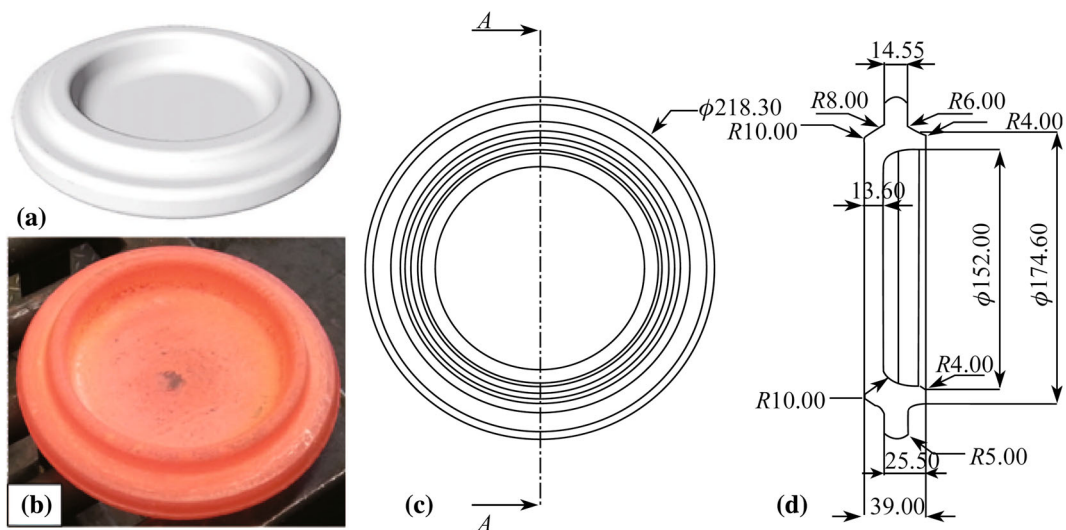


**Fig. 2** Structure of the post-machining **a** 3D view, **b** as forged component, **c** and **d** drawing of the forged component (all dimensions are in mm)

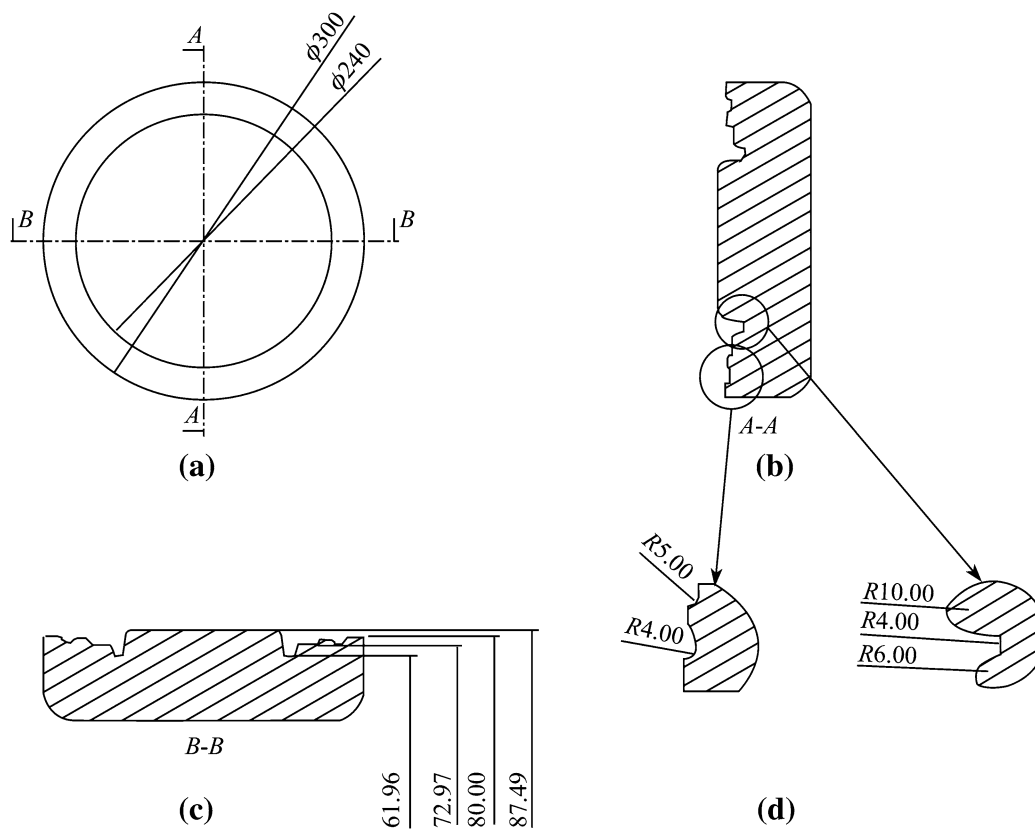


**Fig. 3** Top die geometry **a** top die bottom view, **b** A-A section view, **c** B-B section view and **d** details magnification (all dimensions are in mm)

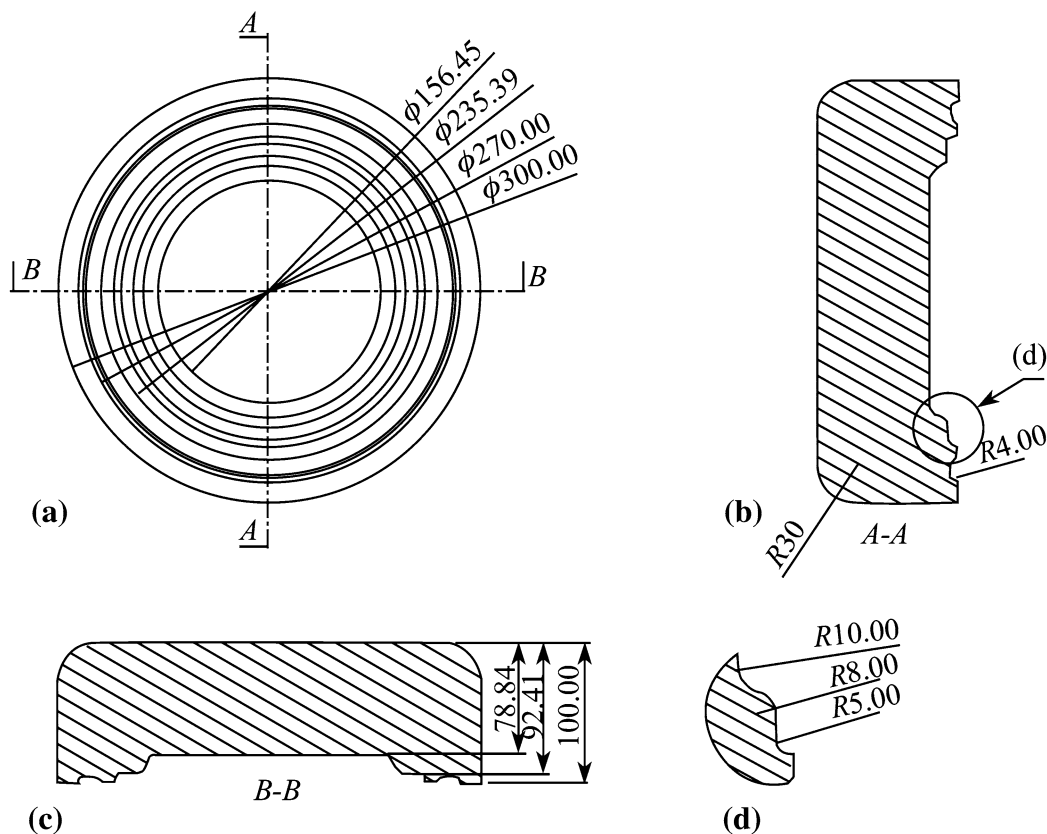


**Fig. 4** Bottom die geometry **a** bottom die top view, **b** A-A section view, **c** B-B section view and **d** details magnification (all dimensions are in mm)

The results of the calibration and experimental campaign were reported in Ref. [24].

## 4 Results and discussion

Four different measuring points were identified for each workpiece in order to extract data concerning the major field variables. Figure 5 shows the position of the tracking points on the cross section of the forged part.

### 4.1 Forging load predictions

Firstly, the forging load was calculated for each considered case study in order to correctly select the forging machine and equipment. The forging load was about 280 t for the 950 °C case study and about 220 t for the 1 050 °C case study (see Fig. 6). A low influence of friction actions on the material flow was observed and a double step curve was obtained because of double cavity on the die. The different loads calculated can be explained considering the temperature affecting the flow stress curve behavior due to different volume fractions of  $\alpha$  phase, which can reach about



**Fig. 5** Position of the four tracking points used for data extraction

20% at 950 °C [25], determining higher mechanical properties of the material.

It is known that the  $\alpha$  phase flow stress is about 3 times greater than that of the  $\beta$  phase [21]. It should be observed that a separate contribution of  $\alpha$  and  $\beta$  phases to the flow stress was not considered in this study.

### 4.2 Temperature prediction

Temperature was calculated in order to analyze the thermal evolution at the tracking points (see Figs. 7 and 8). Both forging and cooling in air stages were considered.

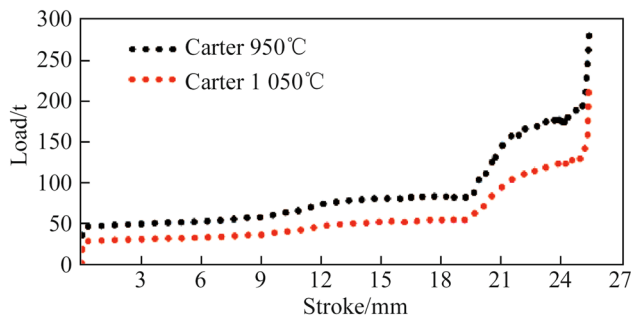


**Fig. 6** Forging load prediction at different billet temperatures

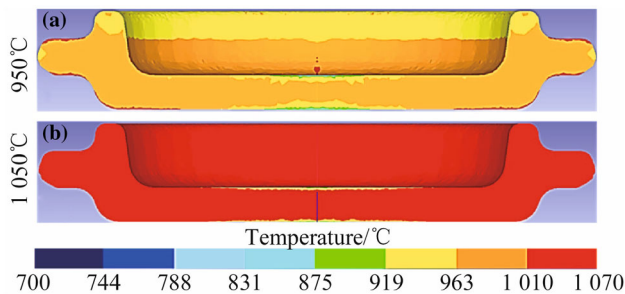


**Fig. 7** Temperature colormap of the cross section of the workpiece at the end of forging stage using **a** 950 °C and **b** 1 050 °C billet temperature

At the end of forging stage, the inner part of the workpiece forged at 1 050 °C is still above the  $\beta$ -transus temperature conditions while the outer surfaces, cooled down due to the contact with the colder dies, are in the  $\alpha$ - $\beta$  region. In these conditions, the high content of  $\beta$  phase determines a forging load lower than the one obtained with a microstructure in which the  $\alpha$  phase content is predominant. This may also lead to flow localization and dynamic heating in the low flow stress  $\beta$ -regions. However, only a small increase in temperature was calculated during the forging stage, with the 950 °C case reaching up to 975 °C and the 1 050 °C reaching up to 1 060 °C, due to the relatively low strain accumulated in the workpiece and the large contact surfaces with dies of the considered geometry (see Fig. 8).

### 4.3 Von Mises strain and strain rate prediction

Effective strain of selected points (see Fig. 9) was calculated in order to predict the deformation of most significant zones and estimate the material flow of the used alloy with varying forging temperature.

Effective strain up to about 1.4 and a double step evolution, which can be related to the load/stroke graph previously shown (see Fig. 6), are observed in Fig. 9.

Looking at the strain colormap (see Fig. 10), a layered trend is highlighted, with the upper zone characterized by

low strain and a central ring undergoing most of the deformation.

As well as effective strain, the effective strain rate of selected points (see Figs. 11 and 12) was calculated in order to predict the deformation rate of most significant zones of each workpiece and evaluate the forgeability by means of comparison with workability maps found in Ref. [26], as it will be explained in the next paragraphs.

The results showed that the effective strain rate calculated for the 950 °C case study, increased during the process. In particular, for points  $P_3$  and  $P_4$ , at the top and bottom of the rib, respectively, values close to  $100 \text{ s}^{-1}$  are calculated at the end of the forging step. This result is due to the adiabatic heating generated during the deformation, causing an increase of the strain-rate with the die stroke.

### 4.4 Phase transformation and volume fraction prediction

The phase evolution of the selected points was studied during the whole process, and the phase distribution along the cross section of the workpiece at the end of both forging and cooling stages was predicted.

The 950 °C case study showed an amount of  $\alpha$  prior phase of about 20%, which remained almost constant during the forging stage (see Figs. 13 and 14), with very small variations caused by the deformation work locally increasing the temperature and, as a consequence, the amount of transformed phase. On the other hand, the  $\beta$  prior volume fraction decreases during the process, because of cooling, causing the  $\alpha$ + $\beta$  transformation (see Figs. 13 and 15).

The 1 050 °C case study showed that the  $\alpha$  prior phase amount was equal to 0 during the entire process due to the higher billet temperature. In this case, the  $\beta$  to  $\alpha$ + $\beta$  phase transformation finishes during the post-forging stage due to the higher heat exchange with environment (see Fig. 16). This is clearly visible in Figs. 17 and 18, in which the color maps of phase distribution show a great amount of  $\beta$  phase in  $P_1$  point after the forging process of the 1 050 °C case study.

### 4.5 Flow instability and forging defects

Strain rate and temperature, numerically calculated at the selected points, were used to analyze the process evolution in a temperature-strain rate domain. A process window coming from literature was used to explain the obtained results. In particular, the values range of both temperature and strain rate, were plotted in the process window coming from a study by Seshacharyulu et al. [13, 26] on workability of Ti-6Al-4V. Using Eqs. (1) and (2), a transition line, separating the safe region from the instable flow one, was identified.

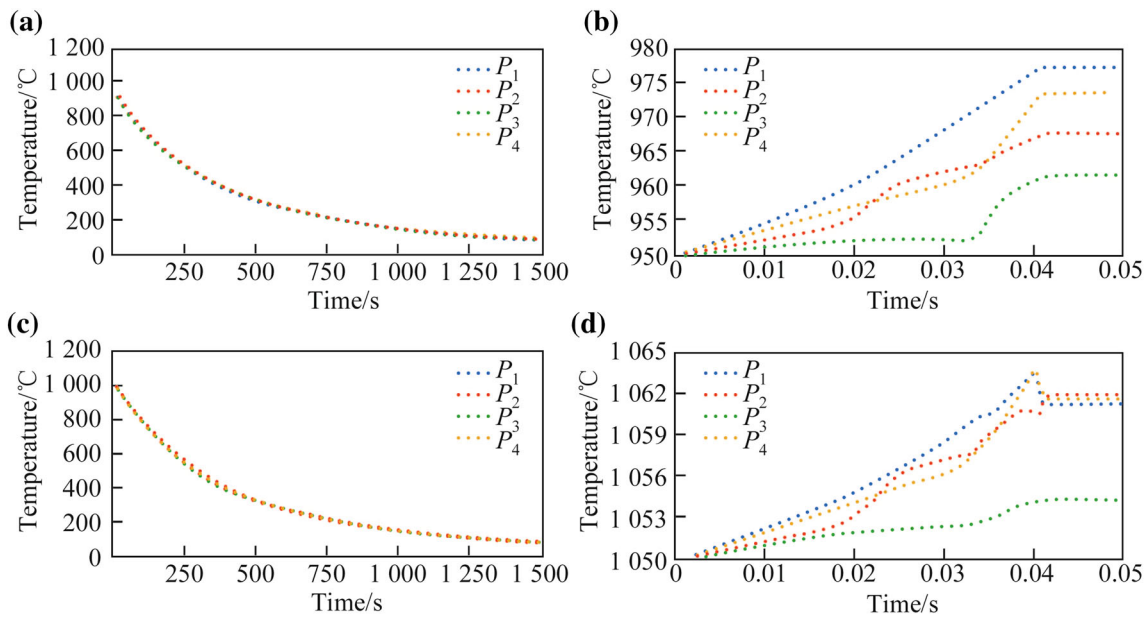


**Fig. 8** Temperature evolution for **a** 950 °C case study, cool down stage; **b** 950 °C case study, forging stage; **c** 1 050 °C case study, cool down stage and **d** 1 050 °C case study, forging stage

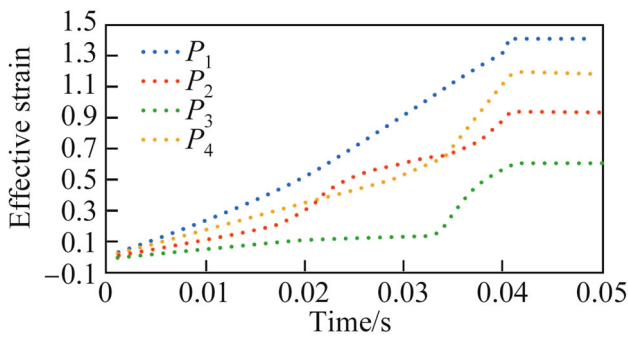


**Fig. 9** Effective strain evolution for the part forged at 950 °C

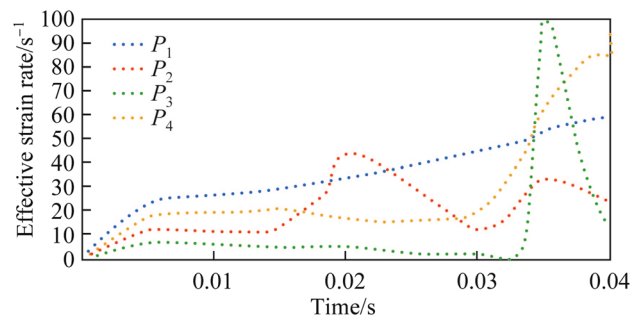


**Fig. 11** Effective strain rate evolution for the part forged at 950 °C

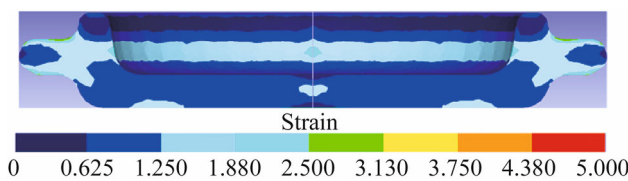


**Fig. 10** Effective strain colormap of the cross section at the end of forging stage for the part forged at 950 °C

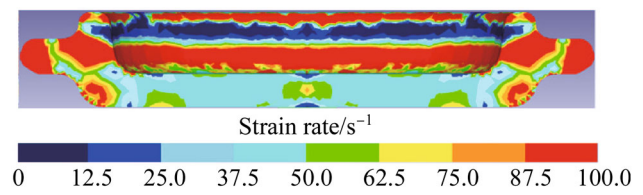


**Fig. 12** Effective strain rate colormap of the cross section at the end of forging stage for the part forged at 950 °C

$$\eta = \frac{2m}{m + 1}, \tag{1}$$

$$\xi(\dot{\epsilon}) = \frac{\partial \ln\left(\frac{m}{m + 1}\right)}{\partial \ln \dot{\epsilon}} + m < 0, \tag{2}$$

where  $\eta$  is the efficiency of power dissipation,  $\xi$  a dimensionless instability parameter and  $m$  the strain rate sensitivity

coefficient which was considered equal to 1.3 (average value of the strain rate calculated during the process).

It is found that the temperature-strain rates of the selected points have almost totally fallen within the safe region in both 950 °C and 1 050 °C cases (Figs. 18–23). Most values are concentrated close to the instability line, which denotes that an increasing in strain rate (or forging speed) may cause instability in material flow. Considering



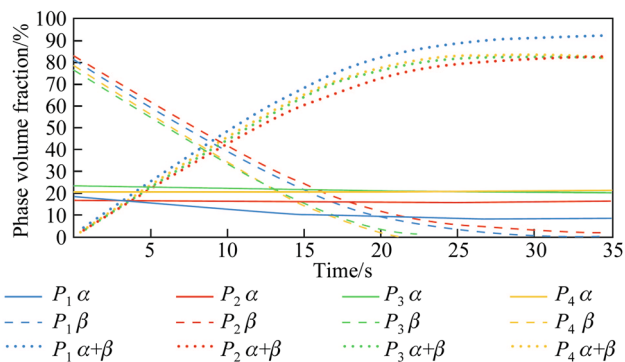


**Fig. 13** Phase volume fraction evolution for the part forged at 950 °C

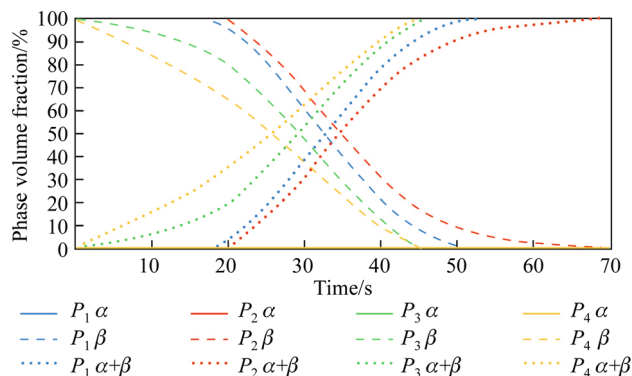


**Fig. 16** Point tracking of phase volume fraction evolution for the case forged at 1050 °C

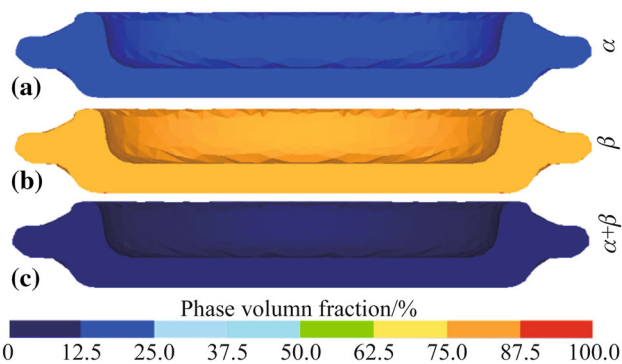


**Fig. 14** a  $\alpha$ , b  $\beta$  and c  $\alpha+\beta$  phase volume fraction colormap at the end of forging stage for the part forged at 950 °C

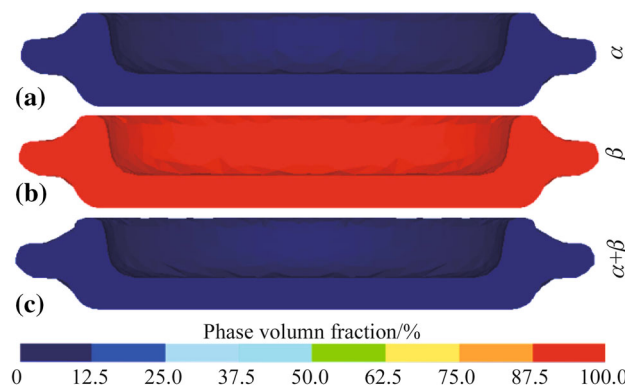


**Fig. 17** a  $\alpha$ , b  $\beta$  and c  $\alpha+\beta$  phase volume fraction colormap at the end of forging stage for the part forged at 1050 °C

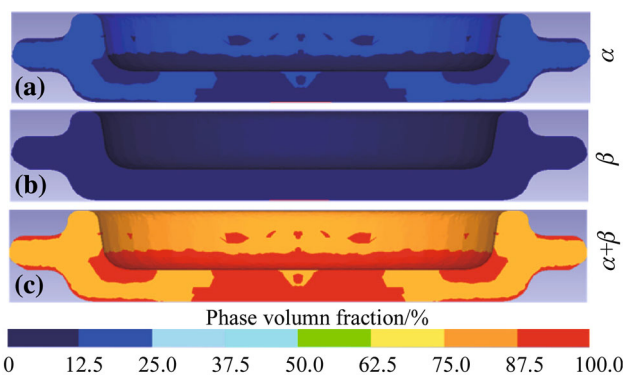


**Fig. 15** a  $\alpha$ , b  $\beta$  and c  $\alpha+\beta$  phase volume fraction colormap at the end of cooling stage for the part forged at 950 °C

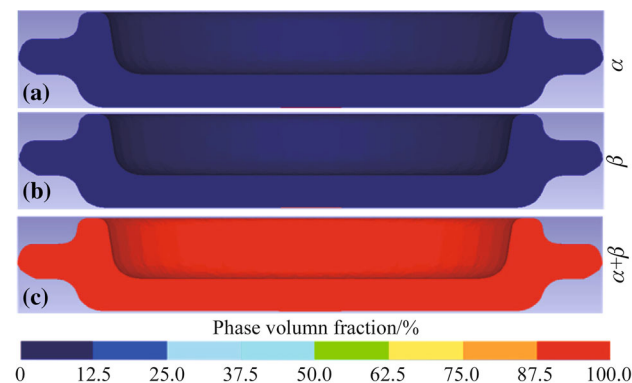


**Fig. 18** a  $\alpha$ , b  $\beta$  and c  $\alpha+\beta$  phase volume fraction colormap at the end of cooling stage for the part forged at 1050 °C

the simulation results, the 950 °C could be improved by selecting a lower value of die speed in order to maintain the strain rate value under the limits identified by the black line.

The instability map prediction was validated by microstructural observations in the  $\alpha$ - $\beta$  regime. The

micrographs do not exhibit flow localization bands formed at an angle of about 45° to the compression axis. This result is justified by strain rate lower than the critical values determined by the instability line in the previous graph (see Fig. 1), as observed in the study conducted by Seshacharyulu et al. [13].

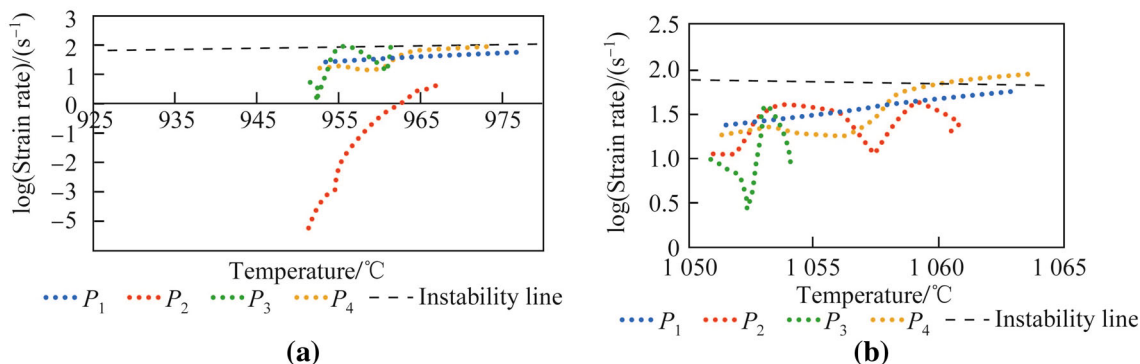


**Fig. 19** Instability map obtained from numerical temperature-strain rate data for the part forged at **a** 950 °C and **b** 1 050 °C (The black line represents the border separating safe and instable zones.)

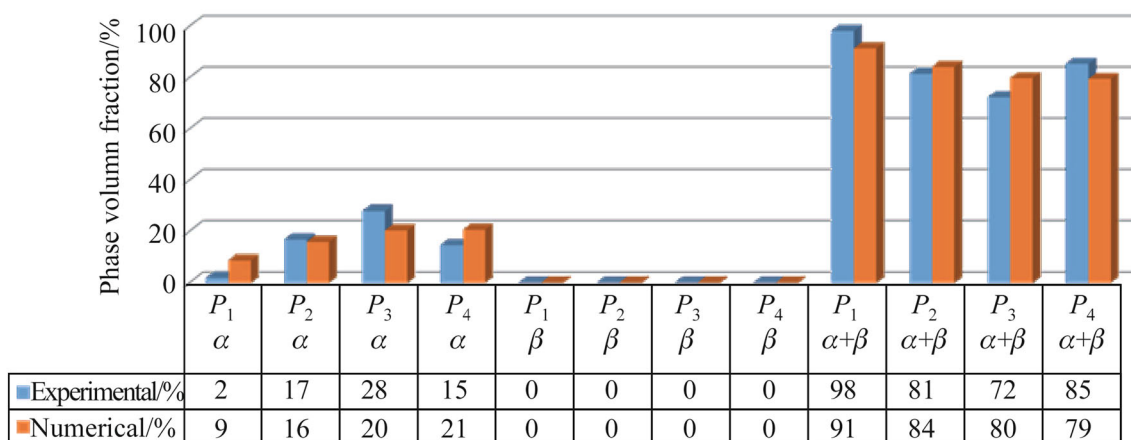


**Fig. 20** Numerical vs experimental comparison of final phase volume fraction at selected points for the part forged at 950 °C

### 4.6 Metallographic analysis

The last step of the validation procedure was the comparison, for each case study, of the calculated final phase distribution with the experimental micrographic analysis on the forged parts.

In order to obtain both qualitative and quantitative information on the phase and volume fraction of the inspected specimens, a dedicated algorithm was created in Matlab™. Further details can be found in Ref. [22].

The utilized procedure includes the following steps:

- (i) Images (size  $M \times N$ ) are firstly decomposed into a grid of  $(m \times n)$  non-overlapping sub-blocks of size  $B \times B$ , where  $m = M/B$  and  $n = N/B$ . The value of  $B$  will be further described in the experimental section.
- (ii) Features are extracted from each sub-block and concatenated to form a  $B \times B \times N_i$  vector, where  $N_i$  is the size of a single block descriptor vector.

- (iii) Feature vectors are then used to train a support vector machine (SVM) used as binary classifier, which is the most used and the simplest solution whenever a binary classification problem has to be solved. The comparison between numerical and experimental data showed a very good agreement in all observed zones of the workpiece. The numerical output demonstrated a fine level of prediction in final phase distribution, and very low differences in percentage of phase amount in the selected points.

The phase prediction shows good accuracy, with an error in microstructure prevision between 1% and 8% for the 950 °C case (see Fig. 20). The micrographic images (see Fig. 2) show that the final microstructure includes lamellar  $\alpha+\beta$  microstructure inside a matrix of globular  $\alpha$  phase. Point  $P_1$  shows an almost complete lamellar  $\alpha+\beta$  microstructure.

The final microstructure of the 1 050 °C case study is characterized by no residual  $\alpha$  prior phase and a complete

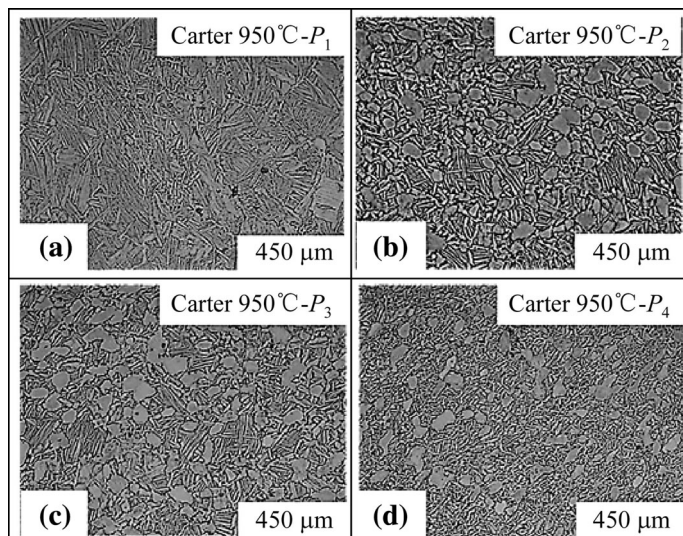


Fig. 21 Micrographic images of a  $P_1$ , b  $P_2$ , c  $P_3$  and d  $P_4$  points of the part forged at 950 °C

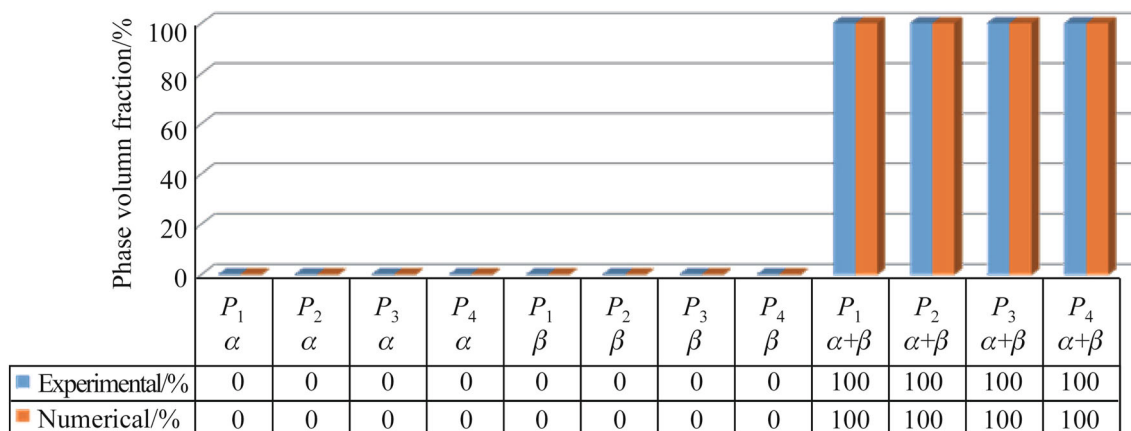


Fig. 22 Numerical versus experimental comparison in final phase volume fraction of selected points for the part forged at 1 050 °C

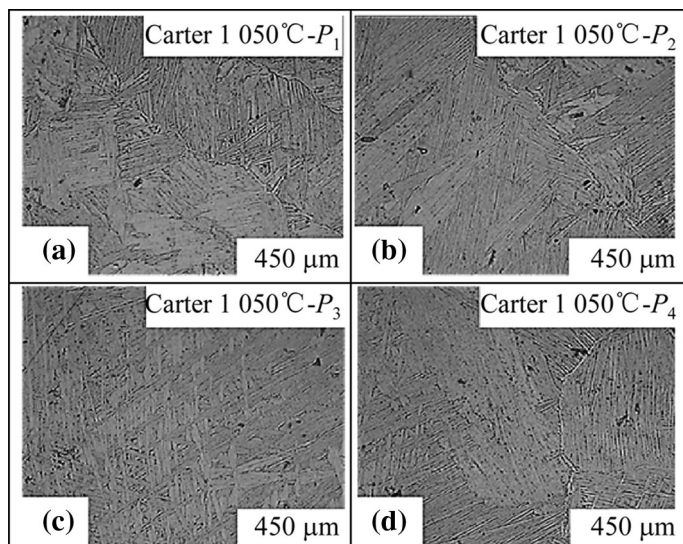


Fig. 23 Micrographic images of a  $P_1$ , b  $P_2$ , c  $P_3$  and d  $P_4$  points of the part forged at 1 050 °C

lamellar  $\alpha+\beta$  morphology (see Fig. 2). This results can be observed also by the micrographic analyses of the selected points (see Fig. 2).

## 5 Conclusions

The forging process of an aeronautical component made of Ti-6Al-4V titanium alloy was simulated by an FE implicit Lagrangian code. The thermo-mechanical-metallurgical characterization of the considered material, previously carried out, was used to calibrate the numerical model and to predict the phase distribution after the process. Two different billet temperatures, above  $\beta$ -transus and below  $\beta$ -transus, were chosen in order to investigate both forgeability and microstructure as function of the thermo-mechanical conditions. The resulting material flow and phase transformations were compared to the experimental forgings through a metallographic analysis of selected points. Additionally, the numerical output in terms of temperature and strain rate was used to examine the flow stability during the forging stage. The following conclusions can be drawn:

- (i) An increase of about 10% of the billet initial temperature, i.e., from 950 °C to 1 050 °C, results in a reduction of more than 20% of the maximum forging load, i.e., from 280 kN to 220 kN. This is due to the phase change occurring in the material.
- (ii) Limited heating is observed in the forged part during the process due to the relatively low accumulated strain and the large surfaces in contact with the colder dies.
- (iii) The final microstructure is mainly  $\alpha+\beta$  with 10%–15% of  $\alpha$  grains for the 950 °C case study. A complete  $\alpha+\beta$  lamellar structure is found for the 1 050 °C case study. Good overlapping was found between the experimental measurements and numerical calculation of phases volume fraction.
- (iv) The use of a temperature-strain rate stability map permitted to assess, starting from the numerical results, that defect free components can be produced with the dies geometry and technological parameters utilized in this project. However, being the points very close to the critical value, further increase of the die speed, i.e., of the strain rate, would result in the presence of flow localization bands.

Future work includes the enhancement of the model by using a different flow stress model considering the separate contribution of both the individual phases, combined with the changes in the phase volume fraction.

## References

1. Kuhlman GW (2005) Forging of titanium alloys. ASM handbook: metalworking. Bulk Forming 14A:331–353
2. Pishko R, Ripepi MA, Kuhlman GW et al (1987) Modeling of deformation and structure during conventional forging of titanium-alloys. J Metals 39(10):A2–A2
3. Boyer RR (1996) An overview on the use of titanium in the aerospace industry. Mat Sci Eng a-Struct 213(1–2):103–114
4. Baufeld B, Biest OVD, Gault R (2010) Additive manufacturing of Ti-6Al-4V components by shaped metal deposition: microstructure and mechanical properties. Mater Design 31:S106–S111
5. Park NK, Yeom JT, Na YS (2002) Characterization of deformation stability in hot forging of conventional Ti-6Al-4V using processing maps. J Mater Process Technol 130:540–545
6. Lutjering G, Williams JC (2003) Titanium matrix composites. Eng Mater Process 2003:313–328
7. Wang J, Fu P, Liu H et al (2012) Shrinkage porosity criteria and optimized design of a 100-ton 30Cr2Ni4MoV forging ingot. Mater Des 35:446–456
8. Bariani PF, Negro DT, Bruschi S (2004) Testing and modelling of material response to deformation in bulk metal forming. Ann Cirp 53(2):573–595
9. Astarita A, Testani C, Scherillo F et al (2014) Beta forging of a Ti6Al4V Component for aeronautic applications: microstructure evolution. Metallogr Microstruct Anal 3(6):460–467
10. Astarita A, Ducato A, Fratini L et al (2013) Beta forging of Ti-6Al-4V: microstructure evolution and mechanical properties. Key Eng Mater 554–557:359–371
11. Ducato A, Fratini L, Micari F (2013) Advanced numerical models for the thermo-mechanical-metallurgical analysis in hot forging processes. AIP Conf Proc 1532(3):3–14
12. Cai J, Li FG, Liu TY et al (2011) Constitutive equations for elevated temperature flow stress of Ti-6Al-4V alloy considering the effect of strain. Mater Des 32(3):1144–1151
13. Seshacharyulu T, Medeiros SC, Frazier WG et al (2000) Hot working of commercial Ti-6Al-4V with an equiaxed  $\alpha+\beta$  microstructure: materials modeling considerations. Mater Sci Eng A 284(1–2):184–194
14. Semiatin SL, Goetz RL, Seetharaman V et al (1999) Cavitation and failure during hot forging of Ti-6Al-4V. Metall Mater Trans A 30(5):1411–1424
15. Hu ZM, Dean TA (2001) Aspects of forging of titanium alloys and the production of blade forms. J Mater Process Tech 111(1–3):10–19
16. Geijselaers HJM, Huétink H (2004) Thermo-mechanical analysis with phase transformations. AIP Conf Proc 712(1):1508–1513
17. Casotto S, Pascon F (2005) Thermo-mechanical-metallurgical model to predict geometrical distortions of rings during cooling phase after ring rolling operations. Int J Mach Tool Manu 45(6):657–664
18. Sha W, Malinov S (2009) Titanium alloys: modelling of microstructure, properties and applications. CRC Press, Woodhead
19. Boyer RF, Welsch G, Collings EW (1994) Materials properties handbook: titanium alloys. ASM international
20. Kim JH, Semiatin SL, Hwan Lee Y et al (2011) A self-consistent approach for modeling the flow behavior of the alpha and beta phases in Ti-6Al-4V. Metall Mater Trans A 42A(7):1805–1814
21. Semiatin SL, Montheillet F, Shen G et al (2002) Self-consistent modeling of the flow behavior of wrought alpha/beta titanium alloys under isothermal and nonisothermal hot-working conditions. Metall Mater Trans A 33(8):2719–2727

22. Ducato A, Fratini L, Cascia ML et al (2013) An automated visual inspection system for the classification of the phases of Ti-6Al-4V titanium alloy. In: Wilson R, Hancock E, Bors A, Smith W (eds) *Computer analysis of images and patterns*, vol 8048. Springer, Berlin Heidelberg, pp 362–369
23. Buffa G, Ducato A, Fratini L (2013) FEM based prediction of phase transformations during friction stir welding of Ti6Al4V titanium alloy. *Mater Sci Eng A* 581(10):56–65
24. Bruschi S, Buffa G, Ducato A et al (2015) Phase evolution in hot forging of dual phase titanium alloys: experiments and numerical analysis. *J Manuf Process*. doi:[10.1016/j.jmapro.2014.12.001](https://doi.org/10.1016/j.jmapro.2014.12.001)
25. Semiatin S, Knisley S, Fagin P et al (2003) Microstructure evolution during alpha-beta heat treatment of Ti-6Al-4V. *Metall Mater Trans A* 34(10):2377–2386
26. Seshacharyulu T, Medeiros S, Frazier W et al (2000) Hot working of commercial Ti-6Al-4V with an equiaxed  $\alpha$ - $\beta$  microstructure: materials modeling considerations. *Mater Sci Eng A* 284(1):184–194